Mass Transfer across Dilated Interfaces

Alexander Tokarz, Marco Millies, and Dieter Mewes
Institute for Process Engineering, University of Hannover, 30167 Hannover, Germany

The mutual dependence of mass and momentum transport at fluid interfaces was studied theoretically and experimentally. Applying thermodynamics of irreversible processes to systems with interfaces showed, on a theoretical basis, that the dilation of the interface acts as a thermodynamic driving force for the mass transfer across the interface. Mass-transfer rates and concentration profiles at the dilated interface between toluene and water were measured using holographic interferometry for various transfer components. Experimental study showed that mass-transfer rates increase with increasing dilational rate, due solely to an enhanced convective transport in the continuous phases. The dilation does not affect the concentrations at the interface. It was demonstrated theoretically that the maximum possible alteration in the interfacial concentrations due to dilation was in the order of magnitude of the experimental accuracy of the interferometer. It was concluded that the thermodynamic driving force due to dilation is — if present — too small to be relevant to technical applications.

Introduction

Interfaces play a significant role for virtually all mass-transfer processes in nature, as well as in industry. The transfer of components across an interface can be subdivided into three steps. Initially, the transferring components are transported to the interface. Successively, they cross the interface and are finally transported away from the interface. In addition, chemical reactions at the interface, as well as in the boundary layers adjacent to the interface, may occur. The transfer rate is such systems is strongly influenced by the physical processes taking place at the interface.

The interface is generally regarded as a two-dimensional (2-D) dividing surface at which all phases are in thermodynamic equilibrium and which moves with the mean velocity of the adjacent continuous phases. However, in reality this is often not the case. The mobility of interfaces may be strongly reduced due to the adsorption of surface active contaminants (tensides). On the other hand, local inhomogeneities of the interfacial tension can lead to strong movements of the interface (Marangoni convection), which consecutively have a great impact on the mass transfer. Liquid/liquid-interfaces are known to exhibit a particularly strong dependence of the mass transfer across the interface on the mobility and the movements of the interface.

Correspondence concerning this article should be addressed to D. Mewes.

The majority of experimental investigations with respect to the role of the interface in the mass-transfer process has been concerned with the interfacial resistance to mass transfer. Differences between the experimentally observed mass-transfer rates and the rates calculated on the basis of both phases being in thermodynamic equilibrium at the interface have been observed in various investigations. Depending on whether the measured mass transfer was reduced or enhanced, the results have been explained often either with an additional interfacial resistance or with interfacial instabilities.

Lewis (1954a,b) investigated a vast number of binary and ternary systems. In his pioneering work he found both reduced and enhanced mass-transfer rates in the experiments in comparison to the theoretically predicted rates. He attributed the reduced transfer rates to the presence of interfacial contaminants, while the enhanced rates were put down to interfacial instabilities. Ward and Quinn (1964, 1965) investigated the transfer of various components across the interface benzene/water and toluene/water, respectively. In their experimental apparatus, the contact time between both phases was well below 0.1 s which resulted in low mass-transfer resistances in the concentration boundary layers in comparison to the experiments of Lewis. However, no interfacial resistance was found. The transfer of acetic acid and propionic acid across the interface toluene/water and *n*-

butanol/water was investigated by Chandrasekhar and Hoelscher (1975). Using an optical Schlieren apparatus, the concentration profiles of the transfering components were measured in a distance of less than 1 mm from the interface. From the experimental results, it was concluded that the largest mass flux of the transferring component does not occur at the toluene/water interface but at a distance of 0.5 mm from the interface. This was attributed to an interfacial resistance. No such phenomena occurred at the *n*-butanol/water interface. An explanation for the unexpected findings was not given. Later, the results were questioned by Huang and Winnick (1976). Harada et al. (1975) measured the mass-transfer rates of various carboxylic acids across a stationary benzene/water interface. No mass-transfer resistance in the interface was found for acetic acid being the transfering component. However, with increasing length of the molecules of the carboxylic acids, the transfer resistance of the interface was found to be no longer negligible. The influence of a momentum transfer at the interface on the interfacial resistance was not considered. Voigtländer et al. (1980) were able to measure the concentration of pyridine as a transfering component within a distance of below 0.66 μm to a toluene/water interface using a radioactive scintillation technique. The found a negligible interfacial resistance as compared to the resistance in the concentration boundary layers. Only with adsorbed contaminants present at the interface, the concentration of the transferring component in the interface approached the concentration at a large distance to the interface and, consequently, the mass transfer was considerably reduced. However, due to the long contact times between the phases (several mixtures), a possible interfacial resistance would have been very difficult to measure.

So far, it has not been clearly proven that two immiscible phases are in thermodynamic equilibrium at the interface regardless of a possible mass or momentum transfer at the interface. This is partly due to the fact that there is no measurement method available to investigate the concentration profiles in the interface during mass or momentum transfer. Even the measurement of concentration profiles in the boundary layers in the immediate vicinity of a moving interface is a difficult task—mainly due to the width of the concentration boundary layers of well below 1 mm.

Modeling of Transport Processes Through Interfaces

For the design of mass-transfer equipment in the industrial practice, the mass transport processes at interfaces are most commonly modeled using either the film theory or the surface renewal theory. The former is originally developed by Whitman and Lewis (1924), the latter by Higbie (1935), however, based on these two models, a large variety of modified equations has been published ever since (for instance, Godfrey and Slater, 1994). Both theories have in common that only the concentration boundary layers adjacent to the interface are modeled, while at the actual interface, thermodynamic equilibrium is assumed. Thus, effects such as those described above are not taken into account. More rigorous models also account for the rheological properties of interfaces. Boussinesq (1913) was among the first who attributed rheological properties such as the interfacial shear viscosity or the interfacial dilational viscosity to an interface. Based on his ideas, there are a number of models where the interface is treated as a separate phase, and the physical behavior of which is mainly controlled by adsorbed molecules (Slattery, 1990; Edwards et al., 1991). In these models, it is assumed that gradients of the interfacial tension exist due to local differences in the number of adsorbed molecules per area interface. These interfacial tension gradients result in shear stresses in the adjacent flow boundary layers which also affect the temperature and concentration boundary layers. Hence, momentum, heat, and mass-transfer processes are hydrodynamically coupled. Attempts have been made to describe interfacial effects such as the Marangoni convection by means of these coupling phenomena (Sternling and Scriven (1959)), however, only with limited success.

An alternative way of considering interfacial transport phenomena is to employ thermodynamics of irreversible processes (TIP). In the TIP, the balance equations for momentum, mass, energy and entropy are incorporated into Gibb's fundamental equation. The resulting equation is of the general form

$$\rho \frac{ds}{dt} + - \operatorname{div} \underline{J_s} + \sigma , \tag{1}$$

where ρ is the density, s is the specific entropy per unit mass, t is the time, $\underline{J_s}$ is the entropy flux, and σ is the produced entropy flow per unit volume. The term on the lefthand side of Eq. 1 denotes the change of entropy per unit volume as a function of time. The first term on the righthand side denotes the divergence of entropy flux across the boundaries of the control volume, and the second term on the righthand side denotes the entropy flow irreversibly produced per unit volume. The produced entropy flow is always greater than zero

$$\sigma \overset{!}{\geq} 0 \tag{2}$$

There are several transport processes which add to the production of entropy within the control volume. The mathematical formulation of the entropy production flow therefore consists of various terms

$$\sigma = \underline{\underline{J_1}} : \underline{\underline{X_1}} + \underline{\underline{J_2}} : \underline{\underline{X_2}} + \cdots + \underline{J_{i-1}} \cdot \underline{X_{i-1}} + \underline{J_i} \cdot \underline{X_i} + \cdots J_{n-1} X_{n-1} + J_n X_n + \cdots \tag{3}$$

Here, J is named "thermodynamic" flux and X is named "thermodynamic force." Both can be either tensorial, vectorial, or scalar. The product of a thermodynamic flux and a thermodynamic force in Eq. 3 is always a scalar. A phenomenological principle of TIP is the existence of a linear relation between all fluxes and forces of the same mathematical order—if the process is sufficiently close to thermodynamic equilibrium

$$J_i = \sum_j L_{ij} X_j \quad \text{for} \quad \forall i, \tag{4}$$

where L_{ij} are phenomenological coefficients. It is due to this principle that in a continuous phase, the energy flux—a vectorial thermodynamic flux—is a function not only of the temperature gradient but also of the concentration gradient, both being vectorial thermodynamic forces. Hence, applying TIP to a system inherently results in a coupling of transport processes. In a continuous phase, the application of TIP leads to the coupling between, for instance, heat and mass transfer as it is known as Soret- or Dufour-effect. In a discontinuous phase, such as an interface, the possible coupling effects are more complex. This has been shown by Bedeaux et al. (1976), Kovac (1977), Hampe (1981), Millies at al. (1994), and Tokarz (1998).

Two-dimensional interface

Bedeaux et al. (1976) and Kovac (1977) apply the TIP to systems with a 2-D interface. The system is shown in Figure 1. Variables in the continuous phases are denoted by the indexes $^+$ and $^-$, respectively. Variables in the interface are denoted by the index ^{s}. Due to the 2-D nature of the interface in this model, transport fluxes with the index ^{s} being perpendicular to the interface are modeled as scalar processes. Transport fluxes with the index ^{s} being parallel to the interface are modeled as vectorial or tensorial processes. If the equations derived by Kovac (1977) are simplified by keeping the velocity in the interface equal to the velocities in the continuous phases on either side of the interface

$$\underline{v}^+ = \underline{v}^- = \underline{v}^s. \tag{5}$$

the following equation for the entropy production flow is obtained

$$\begin{aligned}
\sigma^s = &- \frac{1}{T^s} \overset{\circ}{\underline{\underline{\Pi}}}^{s,sy} : \left[\operatorname{grad} \overset{\circ}{\underline{v}}^s \right]^{sy} \\
&- \frac{1}{T^{s^2}} \underline{J}_q^s \cdot \operatorname{grad} T^s - \frac{1}{T^s} \sum_{k=1}^{n-1} \underline{J}_i^s \cdot \left(T^s \operatorname{grad} \frac{\mu_k^{m,s} - \mu_n^{m,s}}{T^s} \right) \\
&- \frac{\Pi^{sd}}{T^s} \operatorname{div} \underline{v}^s \\
&+ J_{qn}^+ \left(\frac{1}{T^+} - \frac{1}{T^s} \right) + J_{qn}^- \left(\frac{1}{T^s} - \frac{1}{T^-} \right) \\
&- \sum_k \left[\left(J_{kn}^+ + \frac{\rho_k^-}{\rho_k^s} J_{kn}^s \right) \left(\frac{\mu_k^{m,+}}{T^+} - \frac{\mu_k^{m,s}}{T^s} \right) \right. \\
&\left. + \left(J_{kn}^- + \frac{\rho_k^+}{\rho_k^s} J_{kn}^s \right) \left(\frac{\mu_k^{m,s}}{T^s} - \frac{\mu_k^{m,-}}{T^-} \right) \right] \\
&\overset{!}{\geq} 0
\end{aligned} \tag{6}$$

Chemical reactions are not taken into account here. The individual terms can be interpreted as shown in Table 1. From the study of the mathematical nature of the terms in Eq. 6, it is seen that the number of possible couplings of transport processes is larger than in continuous phases, c.f. de Groot and Masur (1962). For instance, the momentum transport due to a dilation or contraction of the interface can be coupled with the heat and mass transfer perpendicular to the inter-

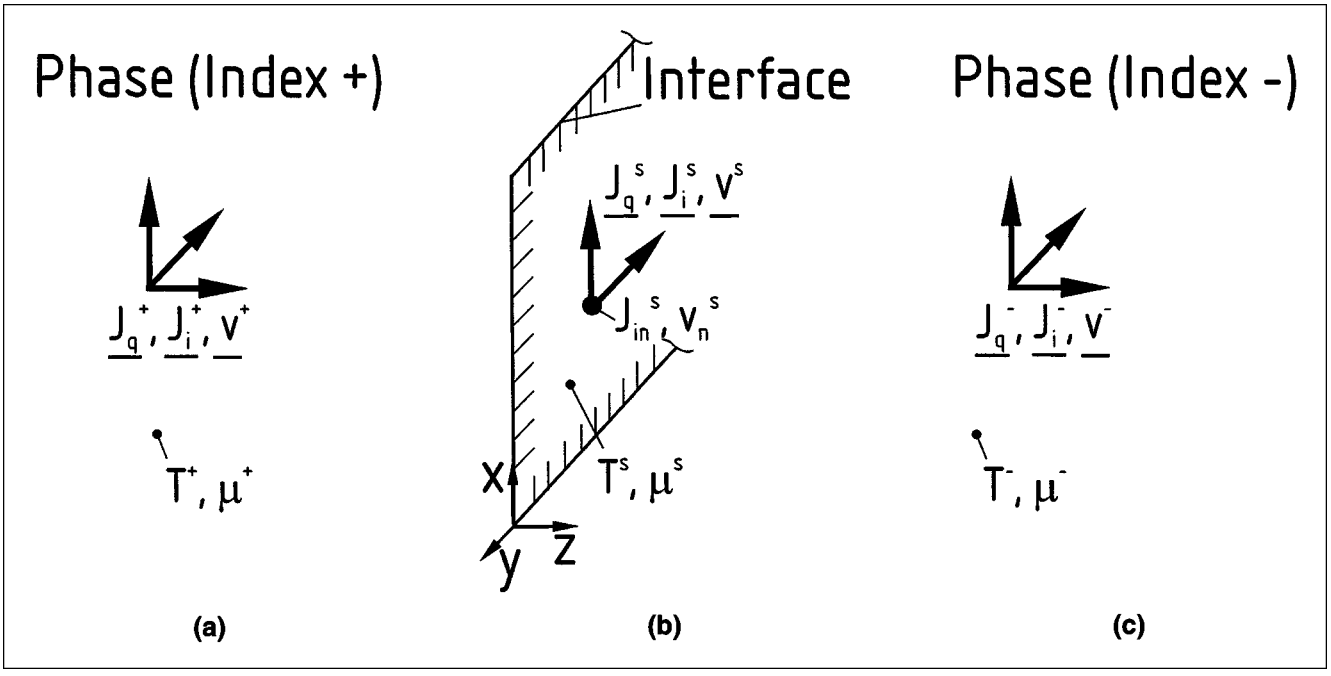

Figure 1. 2-D model of an interface according to Bedeaux et al. (1976).

Table 1. Properties of Systems Studied*

Immiscible liquids Property	Unit	Toluene	Water	Literature
Chem. Eq.		C_7H_8	H_2O	
M	10^{-3} kg/mol	92.14	18.02	
ρ	kg/m^3	860	998	
η	10^{-6} Pa·s	586	1,003	
V_i	m^3/mol	107.1	18.1	
$D_{i,T}$	10^{-9} m^2/s	—	—	
$D_{i,W}$	10^{-9} m^2/s	0.85	—	Ollenik (1983)
γ	10^{-3} N/m	34		Mísek (1978)

Transfer components Property	Unit	Acetone	Acetic Acid	Propionic Acid	Literature
Chem. Eq.		C_3H_6O	$C_2H_4O_2$	$C_3H_6O_2$	
M	10^{-3} kg/kmol	58.08	60.05	74.08	
ρ	kg/m^3	790	1,049	993	
V_i	m^3/mol	73.4	57.2	74.6	
$D_{i,T}$	10^{-9} m^2/s	2.71	2.34*	2.04*	Bulicka (1976), Ward and Brooks (1952)
$D_{i,W}$	10^{-9} m^2/s	1.14	1.04	1.11*	Ollenik (1983) Bulicka and Procházka (1976), Ward and Brooks (1952)
$k = c_{i,T}/c_{i,W}$		$0{,}57 + c_{i,W}\ 10^{-4}$ m^3/mol**	$0{,}013 + c_{i,W}$ $1{,}2\times10^{-4}$ m^3/mol**		Takeuchi and Numata (1977)

*All quantities at 20°C, if not otherwise stated.
**At 25°C.
**At 30°C.

face since all three processes are described by scalar terms. In Eq. 7 the mass flux perpendicular to the interface is given according to the TIP's principle of linear dependence

$$J_{in}^s = \sum_j L_{1j}\left(\frac{\mu_j^{m,+}}{T^+} - \frac{\mu_j^{m,s}}{T^s}\right) + \sum_j L_{2j}\left(\frac{\mu_j^{m,s}}{T^s} - \frac{\mu_j^{m,-}}{T^-}\right) + L_{31}\left(\frac{1}{T^+} - \frac{1}{T^s}\right) + L_{41}\left(\frac{1}{T^s} - \frac{1}{T^-}\right) + L_{51}\underline{\underline{\mathrm{div}}}\,v^s \quad (7)$$

Since the velocity v^s is independent of the z-coordinate perpendicular to the interface, the last term on the righthand side of Eq. 7 can be substituted by

$$\dot{\epsilon} \equiv \underline{\underline{\mathrm{div}}}\,v^s = \frac{\partial v_x^s}{\partial x} + \frac{\partial v_y^s}{\partial y}, \quad (8)$$

$\dot{\epsilon}$ being the dilation rate of the interface. Hence, Eq. 7 expresses a linear relation between the mass flux perpendicular to the interface and the dilation/contraction rate of the interface. This linear relation does not exist in continuous phases.

Three dimensional interface

The TIP is applied to systems consisting of two immiscible phases and a three-dimenionally modeled interface by Hampe (1981), Millies et al. (1994), and Tokarz (1998). In Figure 2 the process of mass transfer of a component i across a plane interface is shown (Millies et al., 1994). A molar flow of the component i is transported from the bulk phase into the interface. The properties of the bulk phase are determined by the concentration of the components. Thus, the molar flux is a function of the gradients of the chemical potentials of all components. It can be described with the known equations for multicomponent diffusion. The properties of the interfacial region are determined by the *structure vectors* a_i of all components i which are a function of the concentration of the components c_i as well as of their gradients. In principle, the structure vector may be of the form

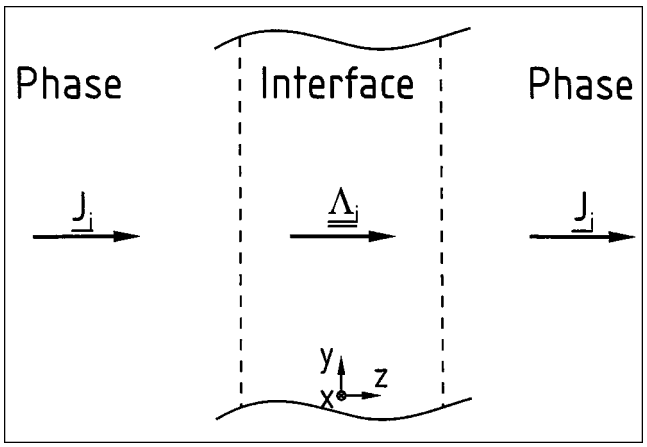

Figure 2. 3-D model of an interface according to Hampe (1981).

$$\underline{a}_i = f\left(c_i, \left[\frac{\partial c_i}{\partial z}\right]^2, \left[\frac{\partial^2 c_i}{\partial z^2}\right], \cdots\right). \tag{9}$$

Note that only even derivatives of the concentration and the square of derivatives determine the structure vector. This is necessary to assure the invariance of the structure vector to the choice of the coordinate system. Within the bulk phase where the concentration gradients are relatively small, the structure becomes identical to the concentration and the well-known transport equations apply. One advantage of the introduction of the structure vector is that location and orientation of an interface are described by a variable for which a balance equation can be formulated. Hence, no *a priori* knowledge about the locus of the interface and the creation or destruction of new interfacial area is necessary. Indeed, the creation of new interfacial area can be described by a process which produces structure. As a result of this model, the mass transport across an interface must be viewed as a structure transport.

From the principles of TIP, the structure transport depends on the gradient of the *interfacial potential* $\underline{\sigma}_i = f(p, T, \underline{a}_i)$, the latter being a vectorial thermodynamic force. To describe the transport of structure of a specific component i, the structure transport tensor $\underline{\underline{\Lambda}}_i$ is defined

$$\underline{\underline{\Lambda}}_i \equiv \underline{a}_i\left(\underline{w}_i - \underline{w}\right). \tag{10}$$

Here, w_i is the velocity of the component i and w is the average molar velocity of all components. Since both the momentum transport and the structure transport are described by second-order tensors, a coupling between the two of them is possible. Millies et al. (1994) show that an equation for the transport of mass similar to Eq. 7 can also be formulated for the 3-D interface

$$J_i^z = \Lambda_i^{zz} = L_{\dot{\epsilon}}\,\kappa(z)\,\dot{\epsilon} - \sum_j T_i^j \frac{\partial a_j^z}{\partial z}. \tag{11}$$

In this equation J_i^z denotes the molar flux and Λ_i^{zz} denotes the structure flux perpendicular to the interface. $L_{\dot{\epsilon}}$ is a phenomenological coefficient, $\kappa(z)$ is the local interfacial dilational viscosity, T_i^j is a transport coefficient for the structure, and a_j^z the z-component of the structure of the species j. The molar flux perpendicular to the interface is a linear function of the dilation rate of the interface, as well as of the structure gradients across the interface. Here, chemical reactions are also not taken into account.

Both, Eqs. 7 and 11 theoretically predict the influence of the dilation of an interface on the mass transfer across the interface. Hence, the coupling between mass and momentum transport expressed in effects such as the Marangoni effect could be related to principles of irreversible thermodynamics. Using the equations of TIP, the transport of matter across interfaces could be described without differentiation between continuous and discontinuous phase.

To allow an experimental verification of the effects predicted by Eqs. 7 and 11, the phenomenological coefficients L_i must be measured since they cannot be derived from thermodynamics. In the present study, therefore, the influence of the dilation of an interface on the mass flux across the interface is measured. To achieve this, the plane interface between the two immiscible liquids toluene and water is dilated in a flow field. The mass transfer of various components across the interface and the concentration profiles in the immediate vicinity of the interface are measured using optical methods. The investigated systems are listed in Table 2 together with their principal properties.

Experimental Setup

In Figure 3 the experimental setup is shown. Both immiscible liquids are kept in two closed storage vessels having an adjustable volume. From these, they are circulated through a flow channel by means of Teflon gear pumps via Teflon tubings. The temperature of the liquids is measured using Pt-100 sensors and controlled by heat exchangers to 0.1 K accuracy.

In Figure 4 the flow channel is illustrated in which both phases are contacted. Along the interfacial contact, the width of the flow cell is constant while its height decreases. This results in an acceleration of the flow and hence a dilation of the entire flow including the interface. The actual interfacial area remains constant. The top and bottom wall profiles are calculated to achieve a constant rate of dilation along the entire interfacial contact. To investigate the interface by optical methods, the flow channel has two glass windows on both sides of the interface. The inner surface of the glass is treated with hexamethyldisilazan to adjust the wetting properties of the surface in such a way that the contact angle between interface and glass is nearly 90°; hence, the meniscus of the interface is as small as possible.

The toluene/water system being investigated is known to be extremely sensitive to surface active contaminants. The

Table 2. Principal Dimensions of the Flow Loops

Flow Loop for the Experiments in the Binary System		Flow Loop for the Interferometric Measurements	
L	100 mm	L	60 mm
B	100 mm	B	22 mm
V_T (Entire loop)	1,685 L	V_T (Entire loop)	0,200 L
V_W (Entire loop)	2,000 L	V_W (Entire loop)	0,200 L
$\dot{V}_T$	0.5…1.5 L/min	$\dot{V}_T$	0,1…0,5 L/min
$\dot{V}_W$	0.6…1.8 L/min	$\dot{V}_W$	0,1…0,5 L/min
$\dot{V}_{rem}$	3…20 mL/min	$\dot{V}_{rem}$	3…20 mL/min
T	20°C	T	20°C

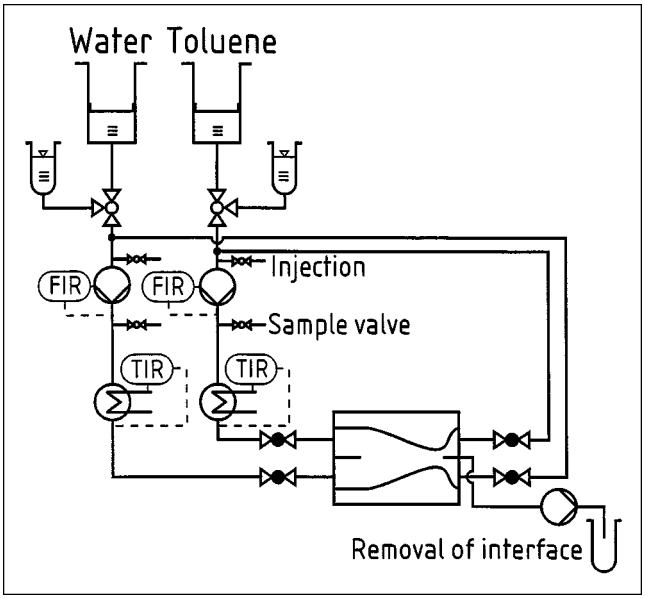

Figure 3. Experimental setup of the flow loop.

latter adsorb at the interface and form a monolayer which greatly reduces the mobility of the interface and, hence, the interfacial dilation. Therefore, the water being used is distilled, washed with activated carbon and filtered through a micropore filter (< 0.45 μm pore size). The organic compounds are of analytical grade. To reduce the elution of surface active contaminants to a minimum, the flow channel and the flow loop only consist of inert material such as stainless steal, Teflon, or glass. The sealings are either from Teflon, Viton, or silicon. However, to prevent remaining contaminants to immobilize the interface, the flow channel is specifically designed to allow the continuous removal of these contaminants from the interface. Using a pump, a small amount —some mL per min—of the two phases including the interface is constantly withdrawn through a 1 mm high slit in the metal partition at the end of the interface. The same amount of liquid is withdrawn from the storage vessels into the loop. The slit is coated with a hydrophobic material (Teflon) at the top and a hydrophilic material (filter paper) at the bottom. The position of the interface is controlled by changing the volume of one storage vessel. Since the entire system is closed, both vessels act as communicating tubes and the position of the interface adjusts accordingly. This way a mobile interface at a constant position is assured for the entire period of time of the experiment.

Table 3. Parameters of the Laser-Doppler-Velocimeter

Laser	Ar-Ionen, $\lambda = 488$ nm
Power in the measurement volume	~ 40 mW
Focal length	121 mm
Fringe spacing	1.2 μm
Size of the measurement volume	Ø 54 μm$\times$300 μm

The velocity of the fluids and the interface are measured nonintrusively using Laser-Doppler-Velocimetry (LDV). The details of the system being used are listed in Table 3. Particles from rutile titandioxide having a mean diameter of 1μm are used as tracer particles. They follow the flow without slip, are chemically inert, and do not emit surface active contaminants.

To determine the mass-flow rate of the transferring component across the interface, the concentrations in both phases are measured. This is carried out by means of spectral photometry in the aqueous phase and gas chromatography in the organic phase.

The principle dimensions and parameters of the flow loop are given in Table 4.

Optical setup

To measure the influence of the dilation on the concentration profiles in the immediate vicinity of the interface, the holographic interferometry is used.

The optical setup being used is shown in Figure 5. The beam of a He-Ne-laser is split into an object and a reference beam. The object beam passes through the flow cell while the

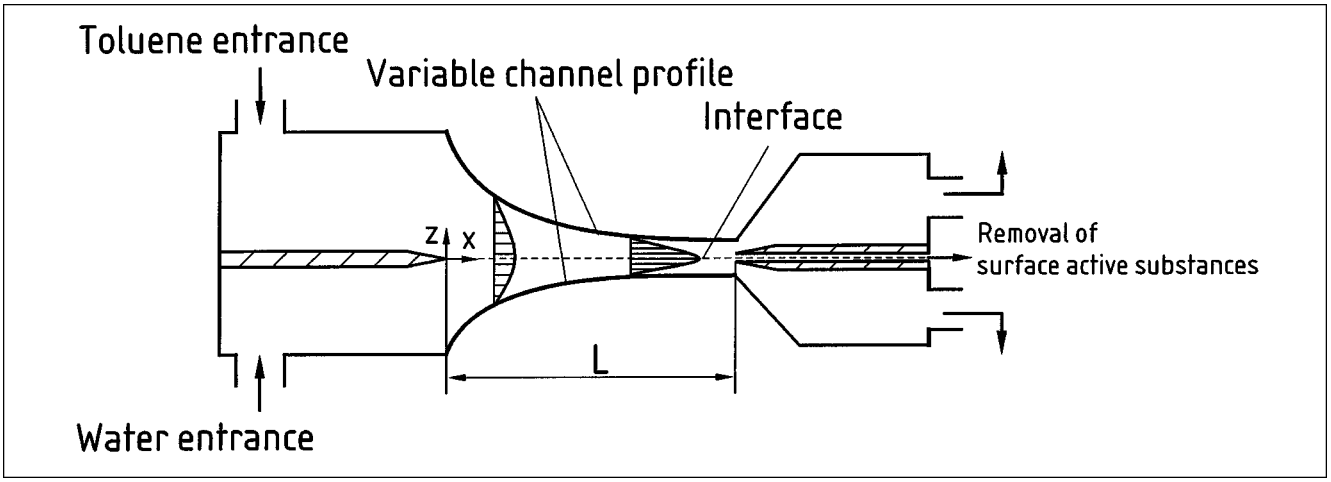

Figure 4. Flow channel for the dilation of the interface.

Table 4. Parameters of the Optical Setup of the Holographic Interferometer

Laser	Helium-Neon, $\lambda = 632{,}8$ nm
Output power	70 mW
Diameter object beam	Ø 100 mm
Diameter reference beam	Ø 20 mm
Focal length viewing optics	135 mm
Type holo plate	AGFA Gevaert 10E75
Size holo plate	127×102 mm
Resolution CCD-camera	512×512 pixel
Lens CCD-Camera	Microscopic lens, 6,3-fold

Table 5. Experimental Parameters

Toluene/Acetone/Water	
Molar fraction of acetone in the mixture, $x_{A,eq}$	0.01…0.3
Dilational rate, $\dot{\epsilon}$	0.1…1 s^{-1}
Toluene/Acetic acid/Water	
Molar fraction of acetone in the mixture, $x_{Aa,eq}$	0.01…0.1
Dilational rate, $\dot{\epsilon}$	0.1…0.5 s^{-1}
Toluene/Propionic acid/Water	
Molar fraction of acetone in the mixture, $x_{Pa,eq}$	0.01…0.1
Dilational rate, $\dot{\epsilon}$	0.1…0.5 s^{-1}

reference beam is transmitted past the flow cell. Using a piezo shifted mirror in the reference beam path, the accuracy of the reconstruction can be enhanced (phase-shift technique). Behind the flow cell, the object and the reference beams interfere on the holographic plate. Using a CCD camera and a frame grabber, the interferograms are recorded in real time. By this procedure, fast phenomena such as the development of interfacial instabilities or concentrations profiles as a function of time can be observed. The parameters of the optical setup are listed in Table 5. A typical interferogram of the concentration boundary layer is shown in Figure 6a. The dark zone at the bottom of the interferogram is due to the blocking of light by the meniscus; the interface forms at the glass windows. The upper limiting line of this dark zone marks the transition between the interface and the continuous phase and is in the following referred to as ''the interface.'' The interference fringes begin approximately 20 μm above the interface and are curved due to the concentration field. The small zone between interface and beginning of interference fringes is influenced by additional diffraction effects and, hence, cannot be evaluated.

For the reconstruction of the interferograms, the phase shift method and the Fourier transformation method are tested. The latter is found to be the favorable method since only one interferogram is needed for a measurement. Hence, small oscillations or movements of the interface during the measurement procedure which cannot be avoided do not act as a source of additional errors. For the Fourier transformation method, a real-time interferogram is recorded using the CCD camera. The interferogram then is transformed from the space domain into the space frequency domain via Fast-Fourier-Transformation (FFT). In the space frequency domain it is filtered and partly transformed back into the space domain. After some mathematical operations, it can be visu-

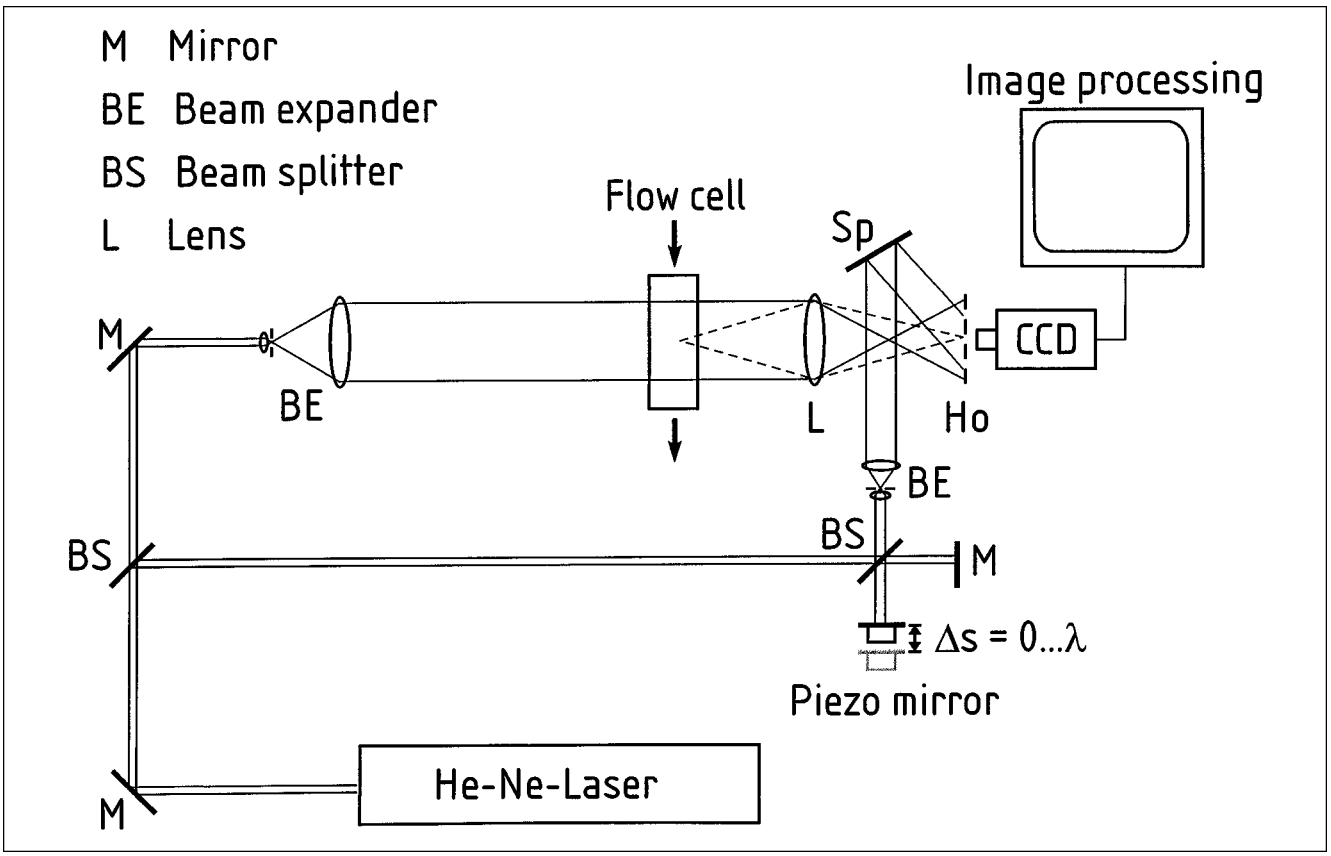

Figure 5. Optical setup for the holographic interferometry.

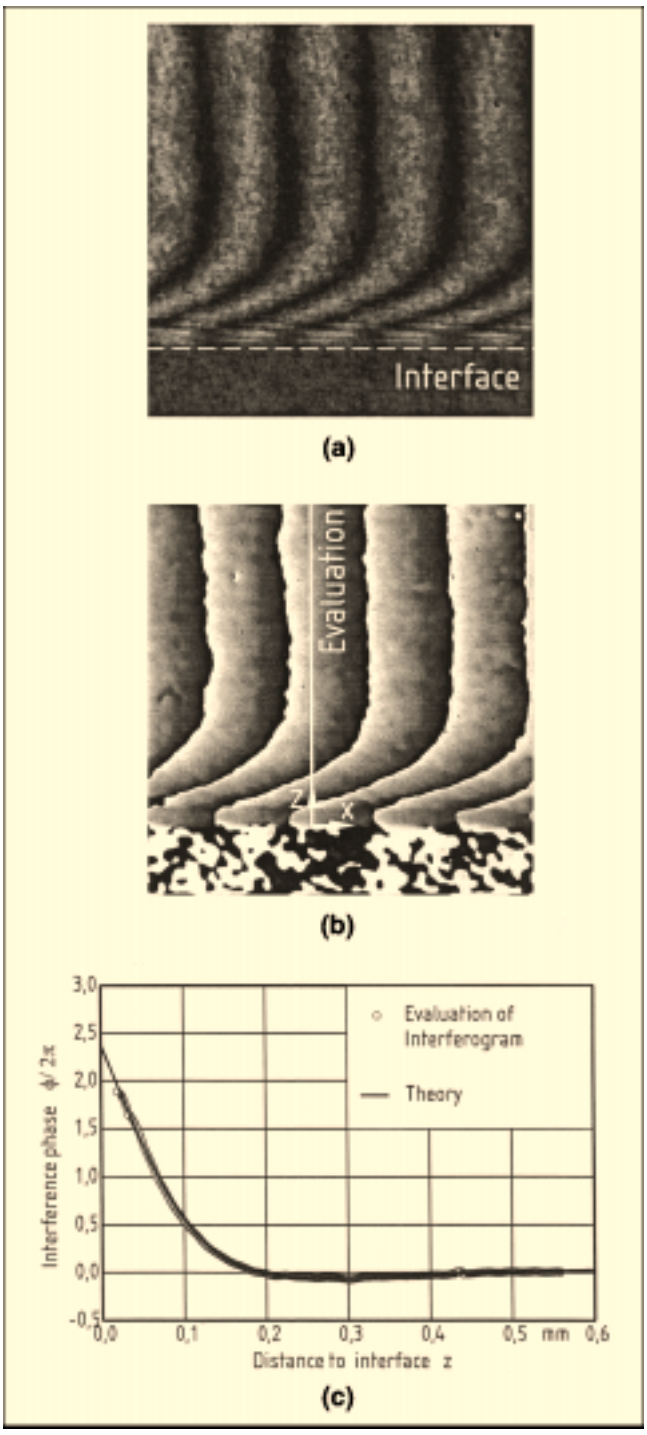

Figure 6. (a) Interferogram of a concentration boundary layer; (b) interference phase after filtration and backtransformation; (c) averaging of the interference phase along the *x*-axis and demodulation.

alized, as seen in Figure 6b. Each gray level represents a value of the phase of the interferogram. The mathematical procedure is described in detail by Kreis (1993) and Tokarz (1998). Due to the periodicity of the phase with respect to 2π, the reconstructed interferogram must be demodulated. The continuous phase profile is then averaged parallel to the interface and plotted as a function of the distance to the interface as shown in Figure 6c. The exact position of the interface marked in Figure 6c is taken from the original interferogram since the transition is blurred by the filtering process. It is assumed that the concentration of all components in the flow channel is constant along the beam path of the object beam. Hence, no concentration profile is present in the *y*-direction. The concentration profiles in the *z*-direction perpendicular to the interface linearly depend on the profile of the interference phase according to the modified principle equation of interferometry

$$\Phi(x,z)\left(\frac{\partial n}{\partial c}\right)^{-1} = c_0(x,z) - c(x,z), \qquad (12)$$

where $\Phi(x,z)$ is the interference phase, $(\partial n/\partial c)$ is the variation of refractive index with concentration and $c_0(x,z)$ and $c(x,z)$ are the concentrations in the reference and the measuring state, respectively.

The proportionality coefficient $(\partial n/\partial c)$ is a property of the fluid and must be known in advance. It may itself be a function of the concentration. The optical properties of the systems being investigated are also given in Table 2. Using holographic interferometry, the concentration of the transferring species can be measured in the immediate vicinity of the interface. Concentration changes at the interface as small as 10^{-3} mol % can be detected in real time.

Results

Experimental results for the flow field

Using LDV, the flow field in the channel is measured. The beam of the LDV is slightly tilted by about 5° with respect to the horizontal to measure the flow velocity in the continuous phase, as well as in the interface. In Figure 7 a plot of the entire flow field in the flow channel is shown. The flow is accelerated along the channel. The interfacial velocity being zero at the position of the first interfacial contact increases due to the acceleration. In Figure 8 a plot of the interfacial

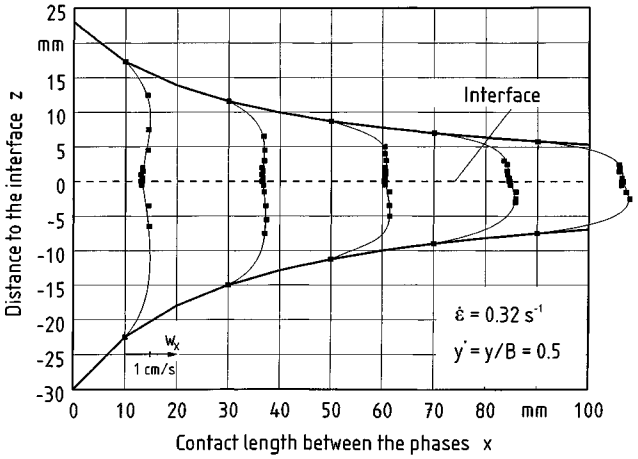

Figure 7. Flow field in the flow channel.

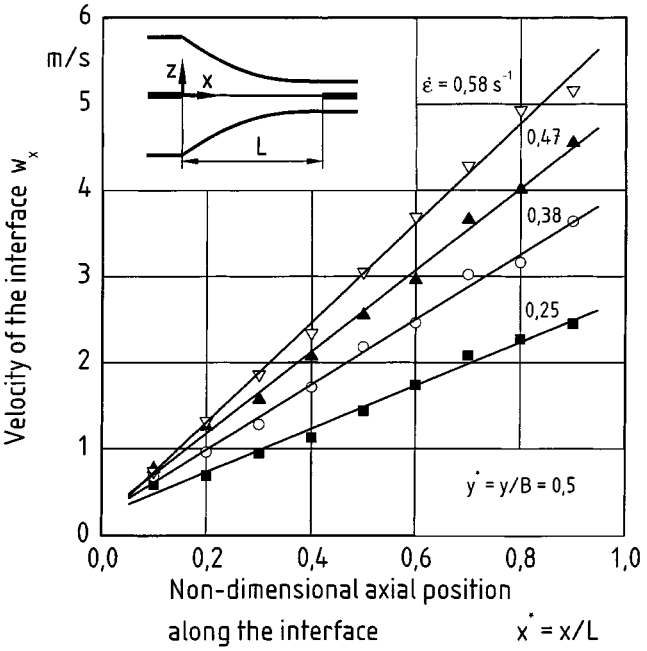

Figure 8. Interfacial velocity as a function of the interfacial contact length.

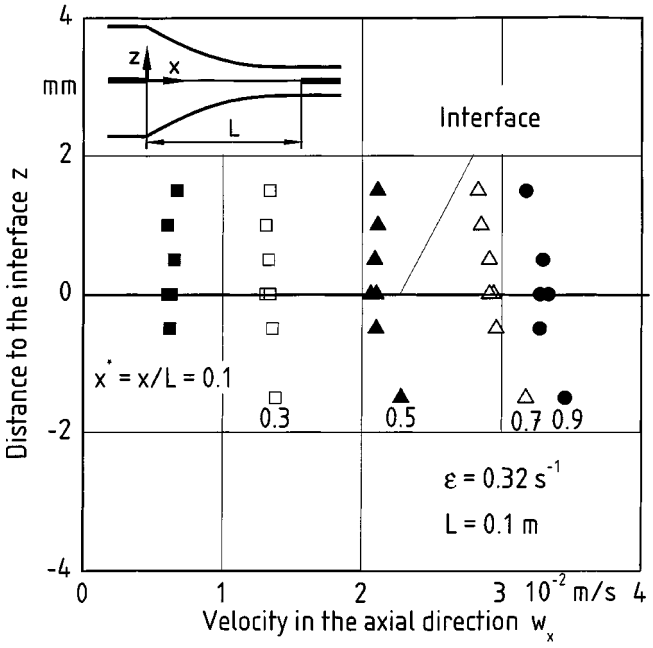

Figure 9. Axial velocity as a function of the distance to the interface.

velocity as a function of the interfacial contact length is shown. The velocity is a linear function of the contact length. Hence, the interfacial dilation rate as given in Eq. 8 is constant. Different dilation rates can be achieved by varying the flow rates of the liquids. The velocity gradient perpendicular to the interface is almost negligible as can be seen from Figure 9. Thus, the shear rate at the interface is comparably small. By continuously removing the interfacial contaminants as described above, a mobile interface could be maintained for the entire period of an experimental run.

Experimental results for the mass transfer: binary system

In preliminary experiments the transfer of toluene from the toluene phase into the aqueous phase is investigated. The transfer rate is calculated as a function of the dilational rate by numerical methods assuming thermodynamic equilibrium at the interface. This is to say that it is assumed that the interfacial concentration of the toluene on the aqueous side $c_{T,W,\mathrm{int}}$ is equal to the equilibrium concentration $c^*_{T,W}(p,T)$, which is dependent on pressure and temperature but not on the dilational rate of the interface

$$c_{T,W\,\mathrm{int}} = c^*_{T,W}(p,T). \tag{13}$$

The concentration field from the numerical calculations is shown in Figure 10 for a dilational rate of 0.44 s^{-1}. The concentration boundary layer on the aqueous side develops rapidly at the beginning of the interfacial contact to reach a constant thickness after about 10 mm. This is in contrast to, for instance, flow above a solid plate. Only at the solid partition at the end of the interface is the flow decelerated near the partition, and the concentration boundary layer suddenly increases in thickness. For the part of the interfacial contact where the thickness of the concentration boundary layer is constant, the mass-transfer rate is also constant. Assuming equimolar mass transfer, which is applicable in the present situation due to the low solubility of toluene in water, the mass-transfer rate can be calculated analytically. From the

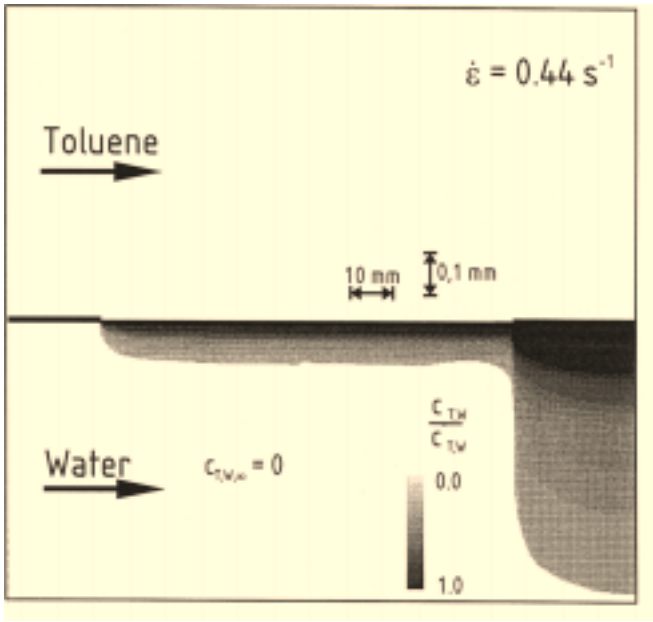

Figure 10. Concentration field for the transfer of toluene in the aqueous phase at a dilation rate of 0.44 s^{-1}.

balance equation of mass for the component toluene

$$\frac{\partial c_{T,W}}{\partial t} + w_x \frac{\partial c_{T,W}}{\partial x} + w_z \frac{\partial c_{T,W}}{\partial z} = D_{T,W}\left[\frac{\partial^2 c_{T,W}}{\partial x^2} + \frac{\partial^2 c_{T,W}}{\partial z^2}\right], \tag{14}$$

the following ordinary differential equation can be derived for the concentration profile (Tokarz, 1998; Tokarz et al., 1998)

$$-\dot{\epsilon} z \frac{\partial c_{T,W}}{\partial z} = D_{T,W} \frac{\partial^2 c_{T,W}}{\partial z^2}. \tag{15}$$

This can be integrated taking into account the boundary conditions to give

$$c_{T,W}(z) = c^*_{T,W} + (c_{T,W,\infty} - c^*_{T,W})\,\mathrm{erf}\left(\sqrt{\frac{\dot{\epsilon}}{2 D_{T,W}}}\, z\right). \tag{16}$$

In the Eq. 16, $c_{T,W,\infty}$ is the concentration of toluene in water at a distance far away from the interface. The mass flux across the interface is given by Fick's law

$$\dot{n}_T = -D_{T,W} \left.\frac{\partial c_{T,W}}{\partial z}\right|_{PG} = (c^*_{T,W} - c_{T,W,\infty}) \sqrt{\frac{2\dot{\epsilon} D_{T,W}}{\pi}}, \tag{17}$$

where $\dot{n}_T$ is the molar flux of toluene across the interface. Using Eq. 17, the mean nondimensional mass flux can be defined in form of a mean Sherwood number

$$Sh = \sqrt{\frac{2}{\pi}} \sqrt{\frac{\dot{\epsilon} L^2}{D_{T,W}}} = \sqrt{\frac{2}{\pi}} \left(Re_{\dot{\epsilon}} Sc\right)^{0,5}. \tag{18}$$

Here $Re_{\dot{\epsilon}} Sc$ can be viewed as a nondimensional dilation rate similar to the convection number. In the experimental investigations, the mass-transfer rate is calculated from the measurement of the concentration of toluene in the aqueous phase as a function of time. The experiments are repeated at various flow rates and dilational rates, respectively. The result of the measurements is shown in Figure 11 as the mean Sherwood number as a function of the nondimensional dilation rate $Re_{\dot{\epsilon}} Sc$. The open circles denote the measurements. The dotted line denotes the calculated values according to Eq. 18. The continuous line indicates the results of the numerical calculations shown in Figure 10; hence, entrance effects, as well as wall effects due to the glass windows, are included. It is seen that both theoretically calculated curves are almost identical. Thus, wall effects and entrance effects obviously cancel out each other. The agreement between measured and calculated mass-transfer rates is good. Therefore, the thermodynamic equilibrium at the interface in this system is not a function of the dilation rate. This is also in agreement with results of Ward and Quinn (1964) who did not find any deviations from thermodynamic equilibrium during mass transfer in the same system.

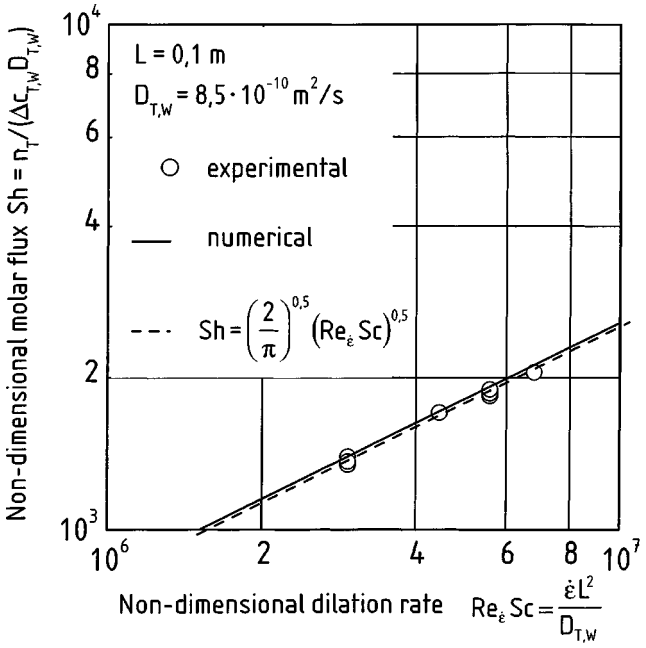

Figure 11. Mean Sherwood number as a function of the nondimensional dilation rate for the transfer of toluene in the aqueous phase.

Experimental results for the mass transfer-ternary system

Similar measurements have been carried out for the transfer of species across an interface in ternary systems. The transfer of acetone, acetic acid, and propionic acid across the toluene/water-interface is examined.

Due to the extremely clean interfaces present at our studies, instabilities are observed even at concentrations being up to one order of magnitude smaller than those published in the past for similar systems (Thornton, 1977; von Reden et al, 1996). Thus, a different approach has been taken. According to the Eq. 7 and 11, the dilational stresses act as driving forces for the mass transfer in accordance with the TIP. This, however, is independent of the presence of another driving force such as a structure or potential gradient. That implies that the effect of dilation on mass transfer occurs, even if both immiscible phases are everywhere in thermodynamic equilibrium, and no concentration profiles, and thus no potential gradients, exist at the nondilated interface. To determine the effect of dilation as a thermodynamic driving force, it is, therefore, possible to measure the deviation from thermodynamic equilibrium due to dilation.

The following equations hold for the transfer of a species A across an interface

$$\frac{c_{A,T,\mathrm{int}}}{c_{A,W,\mathrm{int}}} = k \tag{19}$$

and

$$\dot{n}_{A,T}|_{\mathrm{int}} = \dot{n}_{A,W}|_{\mathrm{int}} \Rightarrow -D_{A,T} \left.\frac{\partial c_{A,T}}{\partial z}\right|_{\mathrm{int}} = -D_{A,W} \left.\frac{\partial c_{A,W}}{\partial z}\right|_{\mathrm{int}}. \tag{20}$$

An equation comparable to Eq. 16 can be derived for the ternary system

$$c_{A,i}(z) = c_{A,i,\text{int}} + (c_{A,i,\infty} - c_{A,i,\text{int}})\,\text{erf}\left(\sqrt{\frac{\dot{\epsilon}}{2D_{A,i}}}\,z\right), \quad \text{with } i = T, W. \tag{21}$$

In Eq. 19, k is the distribution coefficient. Combining Eqs. 19, 20, and 21, it is

$$c_{A,W,\text{int}} = c_{A,W,\infty}\frac{D_A^*}{D_a^* + k} + c_{A,T,\infty}\frac{1}{D_a^* + k} \tag{22}$$

and

$$c_{A,T,\text{int}} = c_{A,W,\infty}\frac{D_A^*}{1 + \frac{1}{k}D_A^*} + c_{A,T,\infty}\frac{1}{1 + \frac{1}{k}D_A^*} \tag{23}$$

with

$$D_A^* = \sqrt{\frac{D_{A,W}}{D_{A,T}}}\,. \tag{24}$$

If the distribution coefficient k is assumed to be dependent on pressure and temperature, but not on the dilation rate, it can be concluded from Eqs. 22 and 23 that the concentrations at the interface $c_{A,W,\text{int}}$ and $c_{A,T,\text{int}}$ do not depend on the dilation rate, with all other parameters being kept constant. However, if Eqs. 7 and 11 are valid, the distribution coefficient is not independent of the dilation rate. Thus, in this case, the concentrations at the interface are dependent on the dilation rate.

As outlined above, the interfacial concentrations in both phases can be measured using holographic interferometry. The experimental procedure is as follows. The two immiscible liquids toluene and water, as well as the transfer component, are brought into thermodynamic equilibrium by mixing all three of them for a certain period of time. Subsequently, the two phases are introduced into the flow rig and circulated through the flow channel at the lowest possible flow rate. While observing the interface in the interferometer, this procedure is continued until thermodynamic equilibrium is again achieved. When thermodynamic equilibrium is reached, the interfacial dilation is initiated. The concentration profiles on either side of the interface are measured using the interferometer. The experiments are carried out for a number of compositions, using acetone, acetic acid, and propionic acid as transfer components.

To quantify the sensitivity of the optical system, at the end of each run, thermodynamic nonequilibrium at the interface is imposed by introducing a known amount of the transfer components into one of the phases and recording the respective interferograms.

In Figure 12 an exemplary set of interferograms for the case of the transfer of acetone is presented. It is obvious that no change with respect to the equilibrium is attained by the dilation. This is found to be the case for all compositions being studied. Similar experiments are performed with acetic acid and propionic acid as transfer components. For these systems, also, no effect of the dilation of the interface on the mass transfer is observed. The parameters of the experiments are listed in Table 5.

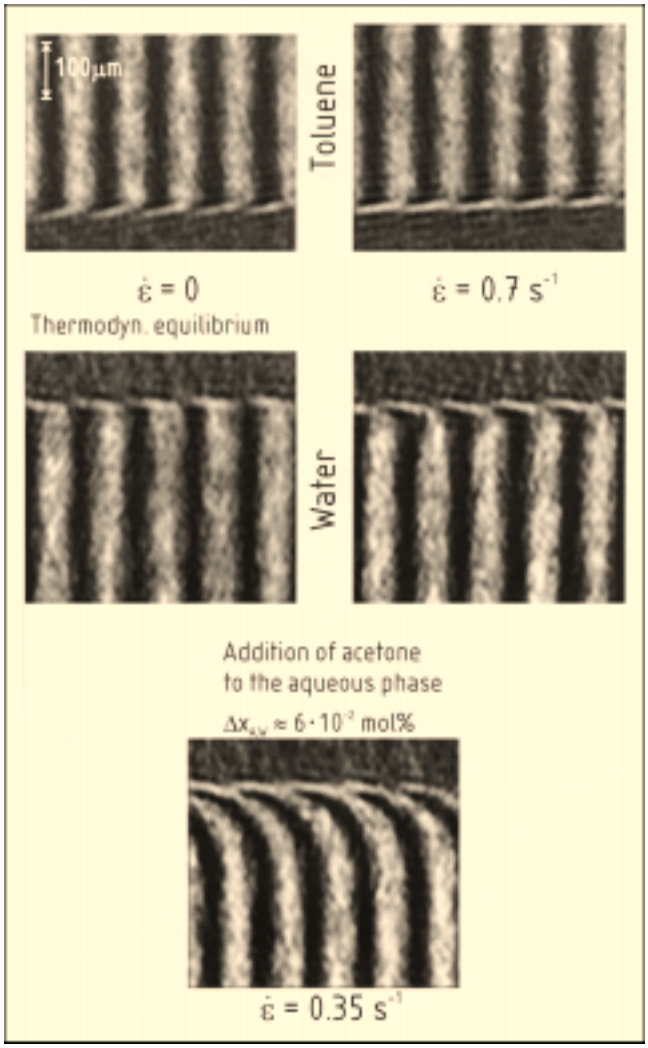

Figure 12. Interferograms of dilated interfaces in the system toluene/acetone/water.

Entropy Balance

There are a number of possible explanations for the experimental results. At first, the influence of the dilation on the mass transfer is solely based upon the models being introduced for the 2-D or 3-D interfaces. The fact that no effect of interfacial dilation on mass transfer has been found suggests that the models may be incorrect. However, there is more likely another possible reason to explain the experimental findings: the effect of the dilation may be too small to result in a measurable deviation from thermodynamic equilibrium. To examine this possibility, the first and second law of thermodynamics for a control volume in the interface as

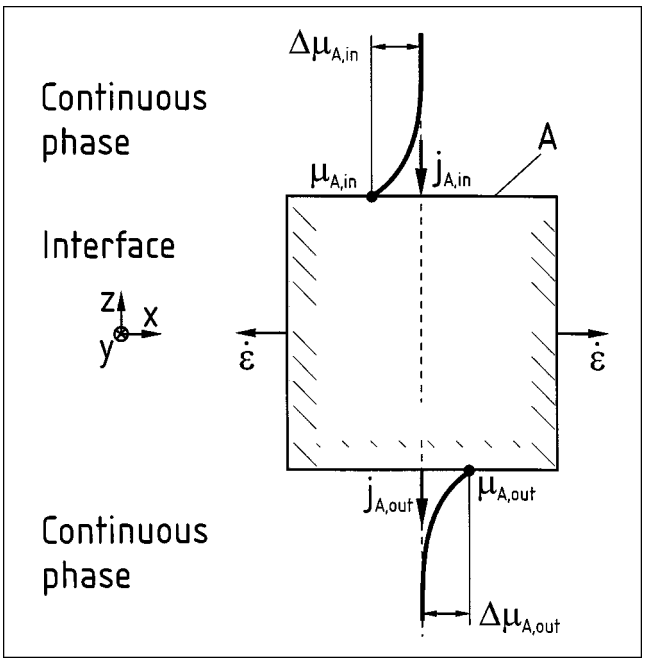

Figure 13. Interfacial volume element.

shown in Figure 13, is formulated. Since the irreversible entropy production in the control volume must be greater than zero, the following equation holds under the assumption of a steady-state situation

$$T\dot{S}_{\mathrm{irr}} = \kappa\dot{\epsilon}^2 A - j_A A(\mu_{A,\mathrm{out}} - \mu_{A,\mathrm{in}}) \overset{!}{\geq} 0. \qquad (25)$$

Here, T is the mean thermodynamic temperature, $\dot{S}_{\mathrm{irr}}$ is the entropy flow due to irreversible processes, κ is the macroscopic interfacial dilational viscosity, A is the area for the mass transfer, j_A is the diffusional molar flux across the boundaries of the element, and $\mu_{A,\mathrm{out}}$ and $\mu_{A,\mathrm{in}}$ are the chemical potential of the component A at the outflow and inflow boundary, respectively.

There are two terms on the righthand side of Eq. 25 describing the production of entropy: the first term denotes the entropy produced by the dilation of the interface against inner forces subsumed by the interfacial dilational viscosity κ. The second denotes the entropy production due to a mass transport through the interface. Using the mean temperature T, the entropy production due to heat transfer is implicitly included in Eq. 25. Equation 25 can be rearranged to give

$$\kappa\dot{\epsilon}^2 \overset{!}{\geq} j_A(\mu_{A,\mathrm{out}} - \mu_{A,\mathrm{in}}). \qquad (26)$$

This equation can be interpreted as follows: At a nondilated interface, the lefthand side of Eq. 26 is zero. Hence, it is

$$\mu_{A,\mathrm{out}} \overset{!}{\leq} \mu_{A,\mathrm{in}}. \qquad (27)$$

If the interface has no resistance to mass transfer, both chemical potentials are equal. Otherwise, the transfer occurs from the higher to the lower chemical potential, as is the case for diffusion in continuous phases.

At a dilated interface, the chemical potential of the ingoing mass flux can be lower than the chemical potential of the outgoing mass flux without violating the second law. The dilation then acts as a thermodynamic driving force necessary to achieve this. Assuming an initial situation of thermodynamic equilibrium, only the deviation of the chemical potential from the equilibrium value $\Delta\mu_A$ must be regarded

$$\kappa\dot{\epsilon}^2 \overset{!}{>} j_A(\Delta\mu_{A,\mathrm{out}} - \Delta\mu_{A,\mathrm{in}}). \qquad (28)$$

This equation can be used to estimate the maximum order of magnitude, the described effect can have without violating the second law. The term on the righthand side of Eq. 28 can be estimated by assuming an appropriate dilational viscosity κ. The term on the lefthand side can be estimated by calculating the minimum value which is measurable by means of holographic interferometry.

The interfacial dilational viscosity must be estimated from literature data since no measurements have been carried out. In contrast to the situation in a continuous phase, the dilational viscosity at interfaces is not negligible (Edwards et al., 1991). This is particularly true for interfaces where a monolayer of surface active molecules is adsorbed. No data are available for the interfacial dilational viscosity at the interface toluene/water; however, Edwards et al. (1991) report that the contribution of the interfacial stress due to dilation of the overall surface tension can be considerable. In absence of specific data, it is assumed that the stresses due to dilation are in the order of magnitude of one percent of the surface tension. This is assumed for an average dilation rate of 0,5 s^{-1}. Thus, it is

$$\kappa \leq \frac{0{,}01\gamma}{\dot{\epsilon}} \approx 7\times10^{-4}\ \mathrm{Ns/m}, \qquad (29)$$

where γ is the surface tension. Although Eq. 29 must be seen as a very crude estimation of the exact value of κ, it serves well as an upper limit for κ. It is very unlikely that the contribution of the dilational stresses to the overall interfacial tension is larger than estimated by Eq. 29. However, it may well be considerably smaller.

To estimate the term on the righthand side of Eq. 28, a number of parameters must be taken into account. It is

$$j_A(\Delta\mu_{A,\mathrm{out}} - \Delta\mu_{A,\mathrm{in}}) = f\left(\lambda, B, \Delta S, \frac{\partial n_A}{\partial c_A}, D_A, \frac{\partial \mu_A}{\partial c_A}, \dot{\epsilon}\right) \qquad (30)$$

The parameters λ, B, ΔS, and $\partial n_A/\partial c_A$ are determined by the optical setup and the optical properties of the system. The parameters D_A and $\partial\mu_A/\partial c_A$ are physical properties of the system. The parameter $\dot{\epsilon}$ is varied in the investigations. The variation of the chemical potential as a function of the concentration $\partial\mu_A/\partial c_A$ is calculated using an NRTL model according to Sørensen and Arlt (1980). With the minimum fringe order being detectable with the interferometer, ΔS is found experimentally to be 0.2. The results of the calculations using the NRTL model for acetic acid and acetone as transfer components and water and toluene as immiscible

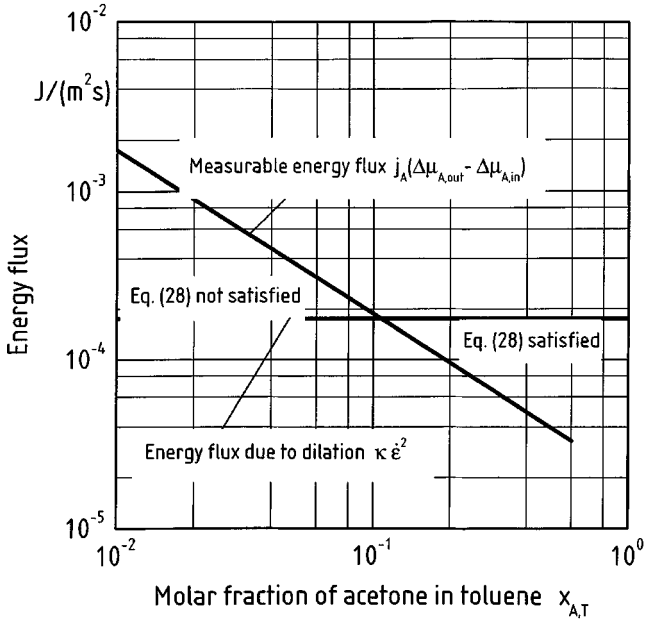

Figure 14. Estimation of the order of magnitude of the effect of dilation.

phases is shown in Figure 14 as the chemical potential gradient with respect to the molar fraction as function of the molar fraction of the transfer component. The results only defer for molar fractions near the plait point.

The results of the estimation of both terms in Eq. 28 is plotted in Figure 14 exemplary for acetone as the transfer component. It is seen that, for fractions below 10 mol % of acetone in the toluene, the measurable potential difference is larger than the maximum possible potential difference. Thus, Eq. 28 is not fulfilled and any effect described by Eqs. 7 or 11 would be undetectable. Only for fractions above 10 mol %, the effect may be measurable. Hence, it can be concluded that the maximum effect that the dilation may impose on the chemical potential profiles at the interface is near the detection level of the used interferometric measurement system. This will be the case for most systems common in liquid/liquid-extraction.

Conclusions

The calculation of mass-transfer rates across interfaces is still restrained by numerous difficulties due to the complex role of the interface in the transfer process. This can be observed, for example, with the Marangoni effect or the restriction of the mobility of an interface due to adsorbed surfactants.

In the present investigations, the thermodynamics of irreversible processes (TIP) is applied for the calculation of mass transfer across interfaces. The interface between two immiscible fluid phases is modeled as a 2-D or 3-D domain, respectively. It is shown that, at interfaces, the coupling between various transport processes predicted by TIP is more manifold in comparison to those in continuous phases. Particularly, it is demonstrated that regardless of the interfacial model, the dilation of an interface acts as a thermodynamic driving force for the mass transfer across the interface.

To verify this experimentally, the mass-transfer and the concentration profiles at the interface between toluene and water are measured for toluene, acetone, acetic acid, and propionic acid as transfer components. The two immiscible liquids are circulated through a flow channel where they form a horizontal plane interface. The flow channel is shaped like a nozzle, so that both liquids as well as the interface are accelerated. The wall profile of the flow channel is calculated to achieve a constant dilation rate of the interface, while the actual interfacial area remains constant. With the aid of laser-doppler-velocimetry (LDV), the velocity profiles in the interface and in its immediate vicinity are measured nonintrusively. From the measurements, it is shown that a constant dilation rate for the entire interface can be achieved. Also, the shear rates are negligible.

Measurements of the transfer of toluene into the aqueous phase show that the mass-transfer rates increase with increasing dilational rates. However, this is shown to be only due to the enhanced convective mass transport in the concentration boundary layer. The experimental results agree well with numerical calculations assuming thermodynamic equilibrium at the interface.

Using holographic interferometry to measure the concentration profiles of transfer components in the immediate vicinity of the interface, deviations from the thermodynamic equilibrium at the interface of below 10^{-3} mol % could be accurately detected. The transfer of acetone, acetic acid, and propionic acid is investigated at molar fractions from zero to 30 mol % and dilational rates of up to 1 s^1. However, no deviation from thermodynamic equilibrium as a result of the dilation of the interface is found.

To estimate the maximum influence possible of the dilation on the thermodynamic equilibrium without violating the second law of thermodynamics, the energy and entropy balance is formulated for an interfacial element. It is theoretically shown that the maximum possible effect is in the order of magnitude of the accuracy of the interferometer found in the experiments. However, due to the uncertainty of the value for the dilational viscosity of the system, the actual size of the effect may be well lower. It is safe to assume, therefore, that the predicted effect of the dilation of an interface on the mass transfer can be neglected in engineering applications.

Acknowledgments

The authors would like to thank the German Research Foundation (''Deutsche Formschungsgemeinschaft'', DFG) which generously provided financial support for the project in its Priority Program ''Transport Phenomena at Fluid Interfaces.''

Notation

B = width of the flow channel, m
j_A = molar flux, $\text{mol}\cdot\text{m}^{-2}\cdot\text{s}^{-1}$
J_k = mass flux of component k, $\text{kg}\cdot\text{m}^{-2}\cdot\text{s}^{-1}$
J_q = heat flux, $\text{W}\cdot\text{m}^{-2}\cdot\text{s}^{-1}$
L = interfacial contact length
$\dot{n}$ = molar flux, $\text{mol}\cdot\text{m}^{-2}\cdot\text{s}^{-1}$
v = velocity, $\text{m}\cdot\text{s}^{-1}$
w = velocity, $\text{m}\cdot\text{s}^{-1}$
x, y, z = coordinates, m
$x_{i,j}$ = molar fraction of component i in phase j
$Re_{\dot{\epsilon}}$ = modified Reynolds number, $= \dot{\epsilon} L^2 \upsilon^{-1}$
Sc = Schmidt number, $= \nu D^{-1}$

Sh = Sherwood number, $= \dot{n}(c^* - c_\infty)^{-1} D^{-1}$
γ = surface tension, $N \cdot m^{-1}$
ΔS = fringe order
$\kappa(z)$ = local interfacial dilational viscosity, $N \cdot s\ m^{-2}$
κ = interfacial dilational viscosity, $N \cdot s\ m^{-1}$
λ = laser wavelength, m
μ_k^m = chemical potential (mass specific partial Gibbs' free energy) of component k, $J \cdot kg^{-1}$
ν = kinematic viscosity, $m^2 \cdot s^{-1}$
Π = stress tensor, $N \cdot m^{-2}$
$=$

Indices

A = acetone
Aa = acetic acid
Pa = propionic acid
eq = equilibrium
int = interfacial
n = normal to the interface
rem = removed
s = in the interface
sy = symmetric tensor
T = toluene
W = water
$+$ = in the continuous phase
$-$ = in the continuous phase
$*$ = thermodynamic equilibrium
∞ = in distance far away from the interface

Literature Cited

Bedeaux, D., A. M. Albano, and P. Mazur, ''Boundary Conditions and Non-Equilibrium Thermodynamics,'' *Physika*, **82a**, 438 (1976).

Boussinesq, J., ''The Application of the Formula for Surface Viscosity to the Surface of a Slowly Falling Droplet in the Midst of a Large Unlimited Amount of Fluid which is at Rest and Possesses a Small Specific Gravity,'' *Ann. Chim. Phys.*, **29**, 357 (1913).

Bulicka, J., and J. Procházka, ''Diffusion Coefficients in some Ternary Systems,'' *J. Chem. Eng. Data*, **21**, 452 (1976).

Chandrasekhar, S., and H. E. Hoelscher, ''Mass Transfer Studies across Liquid-Liquid Interfaces (Use of an Analytical Ultracentrifuge),'' *AIChE J.*, **21,** 103 (1975).

Edwards, D. A., H. Brenner, and D. T. Wasan, *Interfacial Transport Processes and Rheology*, Butterworth-Heinemann, Boston (1991).

Godfrey, J. C., and M. J. Slater, ''Liquid-Liquid Extraction Equipment,'' Wiley, Chichester (1994).

de Groot, S. R., and P. Mazur, *Non-equilibrium Thermodynamics*, North-Holland, Amsterdam (1962).

Hampe, M. J., ''Entropieerzeugende Prozesse an Phasengrenzflächen,'' *Ber. Bunsenges. Phys. Chem.*, **85**, 834 (1981).

Harada, M., T. Imamura, K. Fujioshi, and W. Eguchi, ''Interfacial Resistance in Liquid-Liquid Mass Transfer,'' *J. Chem. Eng. Japan*, **8**, 233 (1975).

Higbie, R., ''The Rate of Absorption of a Pure Gas into a Still Liquid During Short Periods of Exposure,'' *Trans. Amer. Inst. Chem. Engnrs.*, **31**, 365 (1935).

Huang, H. S., and J. Winnick, Comments on: S. Chandrasekhar and H. E. Hoelscher, ''Mass Transfer Studies across Liquid/Liquid Interfaces,'' *AIChE J.*, **21,** 103 (1975), *AIChE J.*, **22,** 205 (1976).

Kovac, J., ''Non-Equilibrium Thermodynamics of Interfacial Systems,'' *Physica*, **86a**, 1 (1977).

Kreis, Th., ''Computer Aided Evaluation of Fringe Patterns,'' *Optics and Lasers in Engineering*, **19**, 221 (1993).

Lewis, J. B., ''The Mechanism of the Mass Transfer of Solutes across Liquid-Liquid Interfaces; Part I - The Determination of Individual Transfer Coefficients for Binary Systems,'' *Chem. Eng. Sci.*, **3**, 248 (1954).

Lewis, J. B., ''The Mechanism of Mass Transfer of Solutes across Liquid-Liquid Interfaces; Part II - The Transfer of Organic Solutes between Solvent and Aqueous Phases,'' *Chem. Eng. Sci.*, **3**, 260 (1954).

Millies, M., St. v. Bose, A. Tokarz, and D. Mewes, ''Einfluß der Dilatation einer ebenen Phasengrenzfläche auf den Stoffdurchgang,'' *Wärme- und Stoffübertragung*, **30**, 17 (1994).

Mísek, T., ''Recommended Systems for Liquid Extraction Studies,'' The Institution of Chemical Engineers, London (1978).

Ollenik, R., ''Laser-Doppler-Messungen an einem flüssig/flüssig-Kanal zur Untersuchung der Wechselwirkungen von Tensidadsorption und -desorption mit Grenzflächenströmung und Stoffaustausch,'' PhD Thesis, TU Munich (1983).

Slattery, J. C., *Interfacial Transport Phenomena*, Springer Verlag Berlin, Heidelberg, New York (1990).

Sørensen, J. M., and W. Arlt, *Liquid-Liquid Equilibrium Data Collection - Ternary Systems*, Chemistry Data Series V/2 DECHEMA, Frankfurt (1980).

Sternling, C. V., and L. E. Scriven, ''Interfacial Turbulence: Hydrodynamic Instability and the Marangoni Effect,'' *AIChE J.*, **5,** 514 (1959).

Takeuchi, H., and Y. Numata, ''The Effect of Interfacial Turbulence on Liquid-Liquid Mass Transfer Rates,'' *Int. Chem. Eng.*, **17**, 468 (1977).

Thornton, J., ''Interfacial Phenomena and Mass Transfer in Liquid-Liquid Extraction,'' *Chemistry and Industry*, 193 (1977).

Tokarz, A., ''Stofftransport durch gedehnte Phasengrenzflächen,'' Fortschritt-Berichte VDI, **3**, 552 (1998).

von Reden, C., M. J. Slater, and A. Gorak, ''Aspects of Multicomponent Mass Transfer Kinetics in Liquid-Liquid-Systems,'' *Proc. of the ISEC*, Melbourne (1996).

Voigtländer, R., H. G. Blaschke, W. Halwachs, and K. Schügerl, ''Investigation of the Mass Transfer across the Interface of Two Concurrent Laminar Flowing Liquids in a Horizontal Cylindrical Channel I,'' *Chem. Eng. Sci.*, **35**, 1211 (1980).

Ward, A. F. H., and L. H. Brooks, ''Diffusion Across Interfaces,'' *Trans. Faraday Soc.*, **48**, 1124 (1952).

Ward, W. J., and J. A. Quinn, ''Diffusion through the Liquid-Liquid Interface,'' *AIChE J.*, **10,** 155 (1964).

Ward, W. J., and J. A. Quinn, ''Diffusion through the Liquid-Liquid Interface: II. Interfacial Resistance in Three-Components Systems,'' *AIChE J.*, **11,** 1005 (1965).

Whitman, W. G., and W. K. Lewis, ''Principles of Gas Absorption,'' *Ind. Eng. Chem.*, **16**, 1215 (1924).

Manuscript received Dec. 23, 1998, and revision received Sept. 20, 2000.